

JGR Space Physics

RESEARCH ARTICLE

10.1029/2019JA026463

Key Points:

- Both the linear theory and 2-D PIC simulations show the WNA and spectrum of excited whistlers is dependent on both hot and thermal electrons
- In high-beta regime, the WNA of the excited dominant whistler is always 0° , which is not affected by thermal electrons
- In low-beta regime, the WNA of the excited dominant whistler turns to 0° from a large value if sufficient thermal electrons exist

Correspondence to:

X. Gao,
gaoxl@mail.ustc.edu.cn

Citation:

Fan, K., Gao, X., Lu, Q., Guo, J., & Wang, S. (2019). The effects of thermal electrons on whistler mode waves excited by anisotropic hot electrons: Linear theory and 2-D PIC simulations. *Journal of Geophysical Research: Space Physics*, 124, 5234–5245. <https://doi.org/10.1029/2019JA026463>

Received 8 JAN 2019

Accepted 18 MAR 2019

Accepted article online 5 APR 2019

Published online 13 JUL 2019

The Effects of Thermal Electrons on Whistler Mode Waves Excited by Anisotropic Hot Electrons: Linear Theory and 2-D PIC Simulations

Kai Fan^{1,2}, Xinliang Gao^{1,2} , Quanming Lu^{1,2} , Jun Guo³, and Shui Wang^{1,2}

¹CAS Key Laboratory of Geospace Environment, Department of Geophysics and Planetary Science, University of Science and Technology of China, Hefei, China, ²Collaborative Innovation Center of Astronautical Science and Technology, Harbin, China, ³College of Mathematics and Physics, Qingdao University of Science and Technology, Qingdao, China

Abstract The wave normal angle of excited whistler waves was previously considered to be controlled by the parallel plasma beta ($\beta_{\parallel h}$) of anisotropic hot electrons, while the effects of thermal electrons were usually neglected. By combining both the linear theoretical and 2-D particle-in-cell (PIC) simulation models, we have investigated the effects of thermal electrons on the whistler anisotropy instability. In the high-beta ($\beta_{\parallel h} \geq 0.025$) regime, the wave normal angle of the dominant whistler mode with the largest growth rate is always 0° , which is not affected by thermal electrons, while, its wave frequency and linear growth rate decrease with the density and temperature of thermal electrons. These results are also confirmed by PIC simulations. In the low-beta ($\beta_{\parallel h} \leq 0.025$) regime, with the increase of the density and temperature of thermal electrons, the wave normal angle of the dominant whistler mode turns to zero from a large value. This change could be due to the stronger damping caused by thermal electrons for oblique whistler mode, since oblique wave usually has a smaller cyclotron resonant velocity than parallel wave. PIC simulations also show a consistent result, but reproduce a broad magnetic spectrum, even in the case including sufficient thermal electrons. Furthermore, thermal electrons with large parallel velocities are resonantly accelerated in the perpendicular direction, while parts of hot electrons are trapped and accelerated in the parallel direction. Our study suggests that the wave normal angle of whistler mode in the Earth's magnetosphere could be determined by both anisotropic and thermal electrons.

1. Introduction

Whistler mode chorus waves are the most intense emissions within the frequency range of $0.1\text{--}0.8f_{ce}$ (f_{ce} is the equatorial electron gyrofrequency) and are also known as chorus waves in the Earth's inner magnetosphere (Burtis & Helliwell, 1969; Li et al., 2012). Whistler mode chorus waves have been widely believed to play an important role in controlling the electron dynamics in the Van Allen radiation belt. They can not only scatter the lower energy (0.1–30 keV) electrons into the atmosphere to cause the diffuse aurora (Ni et al., 2008, 2011; Nishimura et al., 2013; Thorne et al., 2010) but also accelerate the seed electrons (hundreds of keV) up to relativistic energies (approximately MeV) to refill the radiation belt during magnetic storms (Reeves et al., 2013; Thorne et al., 2013; Xiao et al., 2014). Whistler mode waves in the magnetosphere often exhibit a banded structure in the spectrogram, which are separated into two bands (i.e., lower and upper bands) by a power minimum at about $0.5f_{ce}$ (Gao, Lu, et al., 2016; Li et al., 2012; Ratcliffe & Watt, 2017; Tsurutani & Smith, 1974). Many observations have demonstrated that the main source region of whistler mode waves is located near the magnetic equator within a narrow range of magnetic latitudes ($\sim \pm 5^\circ$; Lauben et al., 2002; LeDocq et al., 1998; Santolik et al., 2005). Whistler waves in the magnetosphere, especially lower band waves, are considered to extract the free energy from the anisotropic hot electrons injected from the plasma sheet (Fu et al., 2014; Gao et al., 2014a; Ke et al., 2017; Li et al., 2010; Lu et al., 2004, 2010).

Most of the whistler mode waves in the magnetosphere have a very small wave normal angle (less than 10° ; Li et al., 2013), but there is also a secondary population with a large wave normal angle (Gao, Mourenas, et al., 2016; Li et al., 2013; Santolik et al., 2009). Moreover, whistler mode waves with a finite wave normal angle exhibit some interesting features, distinct from parallel wave characteristics. Such lower band oblique whistler mode wave has a strong electrostatic component, which can couple with its electromagnetic component to drive the upper band harmonic wave (Gao, Lu, et al., 2016; Gao et al., 2018). This lower band cascade mechanism is proposed to explain the generation of multiband chorus waves (Chen et al., 2017; Gao,

Table 1
Some Initial Parameters in These Simulation Runs^a

Parameter	Run 1	Run 2	Run 3	Run 4
$\beta_{\parallel h}$	0.5	0.5	0.012	0.012
A_h	3.0	3.0	9.0	9.0
$\beta_{\parallel t}$	0	0.25	0	0.006
n_t/n_{total}	0	90%	0	80%
$L_{\parallel}(L_{\perp})/\lambda_e$	48.0	51.2	14.0	20.0
$\Omega_e \Delta t$	0.02	0.04	0.02	0.02
$n_x(n_y)$	128	256	128	128
n_p	10,000	500	10,000	10,000

^aThese parameters include the parallel plasma beta of hot electrons $\beta_{\parallel h}$, temperature anisotropy of hot electrons A_h , parallel plasma beta of thermal electrons $\beta_{\parallel t}$, proportion of thermal electrons n_t/n_{total} , simulation box size in x and y direction $L_{\parallel}(L_{\perp})/\lambda_e$, time step $\Omega_e \Delta t$, number of cells $n_x(n_y)$ in x and y direction, and number of macroparticle n_p in each cell for each species.

Lu, et al., 2016, Gao, Ke, et al., 2017, Gao et al., 2018). Similarly, two non-parallel lower band chorus waves can also be coupled with each other, thereby generating a more oblique upper band wave (Fu et al., 2017; Gao, Lu, et al., 2017). Since there are considerable parallel fluctuating electric fields for oblique whistler waves, the Landau resonance also plays an important role in scattering electrons with energies of tens of keV (Agapitov et al., 2015; Artemyev et al., 2016; Shprits & Ni, 2009). Both theory and observations also indicate that oblique whistler waves cause the efficient pitch angle scattering loss of electrons through higher-order cyclotron resonances (Artemyev et al., 2014; Li et al., 2014; Mourenas et al., 2012).

Previous studies considering an electron population consisting of only one (hot) component have shown that the wave normal angle of excited whistler waves is mainly controlled by the parallel plasma beta ($\beta_{\parallel h}$) of anisotropic hot electrons (An et al., 2017; Gary et al., 2011; Yue et al., 2016). Based on the kinetic linear theory, Gary et al. (2011) pointed out

that the dominant whistler mode with the maximum growth rate is parallel propagating if $\beta_{\parallel h} > 0.025$, while the maximum growth rate shifts to oblique propagation if $\beta_{\parallel h} < 0.025$. This critical value of plasma beta is then supported by a statistical work conducted by Yue et al. (2016), where they found quasi-parallel and oblique lower band chorus waves are roughly separated by $\beta_{\parallel h} = 0.025$. The two-dimensional (2-D) particle-in-cell (PIC) simulations also give results that are consistent with the linear theory (An et al., 2017). However, in above theoretical and simulation works, the plasma only includes one electron component, that is, anisotropic hot electrons, but there are typically at least two components of electrons (thermal and hot electrons) in the Earth's magnetosphere (Fu et al., 2014; Gao et al., 2014a; Li et al., 2010). Moreover, the statistical results by Yue et al. (2016, Figure 3 therein) indicate that there are also some quasi-parallel lower band whistler waves with very small wave normal angles below $\beta_{\parallel h} = 0.025$. Therefore, in this paper, we try to investigate the effects of thermal electrons on the whistler anisotropy instability by employing both the linear theory and 2-D PIC simulation model. Interestingly, we find that under certain conditions, the existence of thermal electrons greatly change the wave normal angle distribution of excited whistler mode waves besides the reduction of the growth rates.

The rest of this paper is organized as follows. Both linear theoretical and PIC simulation models used in this study are described in section 2. The results are presented in section 3. At last, we summarize the principal results and give some related discussions in section 4.

2. Linear Theoretical and PIC Simulation Models

In this paper, we try to study the effects of thermal electrons on whistler waves excited by anisotropic hot electrons in a homogeneous plasma by a combination of the linear theory and PIC simulations. The WHAMP (Waves in Homogeneous Anisotropic Magnetized Plasma) model (Ronnmark, 1982) is chosen to calculate the dispersion relation and linear growth rates, which has been widely used in previous works (Xiao et al., 2007; Chen, Gao, Lu, Sun, et al., 2018, Chen, Gao, Lu, & Wang, 2018; Denton, 2018). This code can be easily accessed on <https://github.com/irfu/whamp>. In each case, there are generally three components (i.e., protons, thermal electrons, and hot electrons) in the plasma system, which are denoted by subscripts i , t , and h hereafter, respectively. The anisotropy is defined by the ratio between the perpendicular and parallel temperatures with respect to the background magnetic field for each component. Both protons and thermal electrons satisfy isotropic Maxwellian velocity distribution, while the velocity distribution of anisotropic hot electrons is bi-Maxwellian with $T_{h\perp}/T_{h\parallel} > 1$. In all cases, the ratio of electron plasma frequency and gyrofrequency (ω_{pe}/Ω_e) is fixed as 4, which is a reasonable value in the inner magnetosphere (Gao et al., 2014b). To perform one linear theory calculation, we need to initialize some parameters in the WHAMP model, such as the density, parallel beta, and anisotropy of each component, and ω_{pe}/Ω_e .

The PIC simulation model is a powerful tool to study plasma waves in a self-consistent system (Chen, Gao, Lu, Sun, et al., 2018; Fu et al., 2014; Gao, Ke, et al., 2017; Ke et al., 2017, 2018), where the electromagnetic

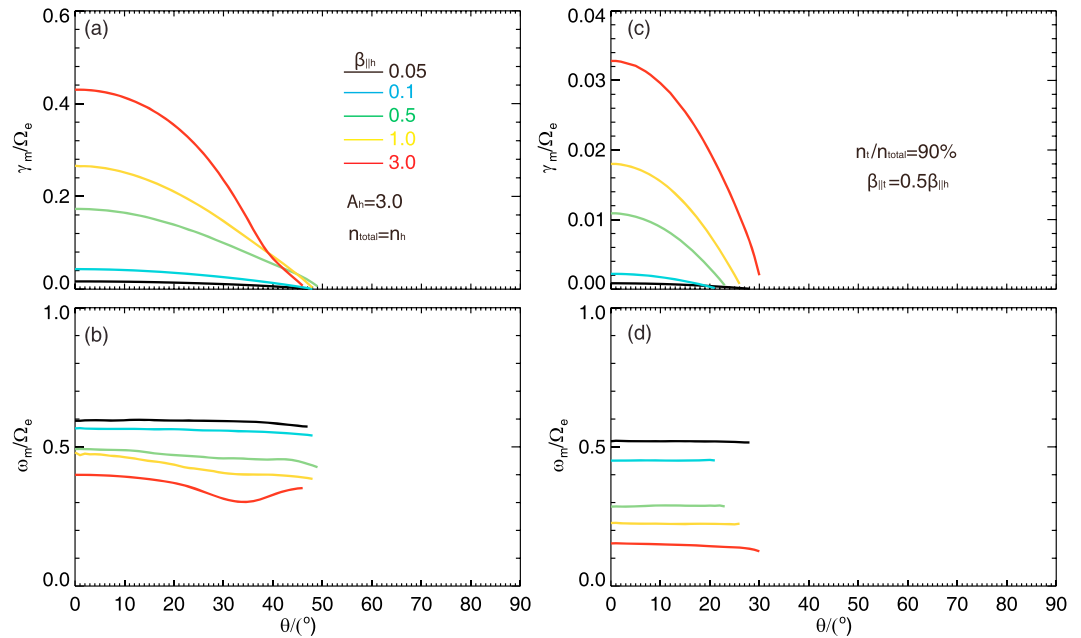


Figure 1. (a, c) The linear growth rate γ_m and (b, d) frequency ω_m as a function of wave normal angle for a series of cases with different parallel plasma betas in the high-beta regime. In each case, γ_m and ω_m denote the growth rate and frequency of the wave mode with the maximum linear growth rate at each wave normal angle.

fields are updated by solving Maxwell equations and the positions and velocities of ions and electrons are advanced by solving relativistic motions in the electromagnetic fields. This model includes the full three-dimensional electromagnetic fields and velocities but only allows spatial variations in x and y directions. The background magnetic field \mathbf{B}_0 is along the x axis. In this model, the periodic boundary condition is adopted. Note that the protons are simply treated as a fixed positively charged background by setting the mass ratio between proton and electron (m_i/m_e) as infinity. Here space and time are normalized to the electron inertial length $\lambda_e = c/\omega_{pe}$ and inverse of electron gyrofrequency Ω_e^{-1} , respectively. In this study, we have carried out four runs, and the initial setup for each run has been listed in Table 1.

3. Results

3.1. Linear Theoretical Results

Since the parallel plasma beta of hot anisotropic electrons $\beta_{||h}$ is a key factor controlling the wave normal angles of excited whistlers, we investigate the effects of thermal electrons for cases classified into two regimes (high-beta [$\beta_{||h} > 0.025$] and low-beta [$\beta_{||h} < 0.025$]) with the WHAMP model. Note that the parallel plasma beta is defined by $\beta_{||j} = 2\mu_0 n_e k_B T_{||j} / B_0^2$ (where j represents different species and n_e is the total electron density) in our study.

Figure 1 shows (a, c) the linear growth rate γ_m and (b, d) frequency ω_m as a function of wave normal angle for a series of cases with different parallel plasma betas in the high-beta regime. Here γ_m and ω_m denote the growth rate and frequency of the wave mode with the maximum linear growth rate at each wave normal angle. In Figures 1a and 1b, there are only anisotropic hot electrons in those cases, while there is a thermal component ($\beta_{||t} = 0.5\beta_{||h}$) accounting for 90% of total electrons in cases presented in Figures 1c and 1d. In Figure 1a, we find that the dominant whistler mode with the largest growth rate for each case is always parallel propagating in

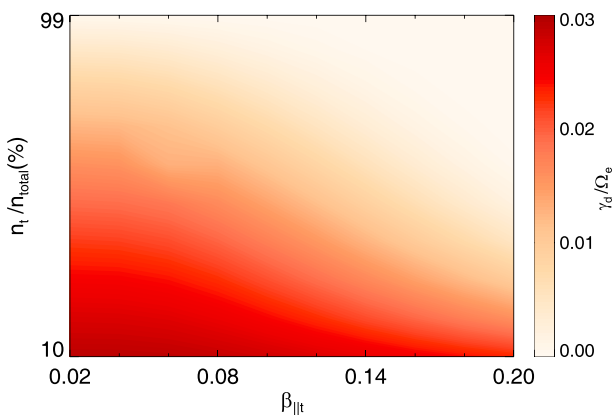


Figure 2. The distribution of the linear growth rate γ_d in the $(\beta_{||t}, n_t)$ plane in the high-beta regime. Here γ_d represents the linear growth rate of the dominant wave mode in each case.

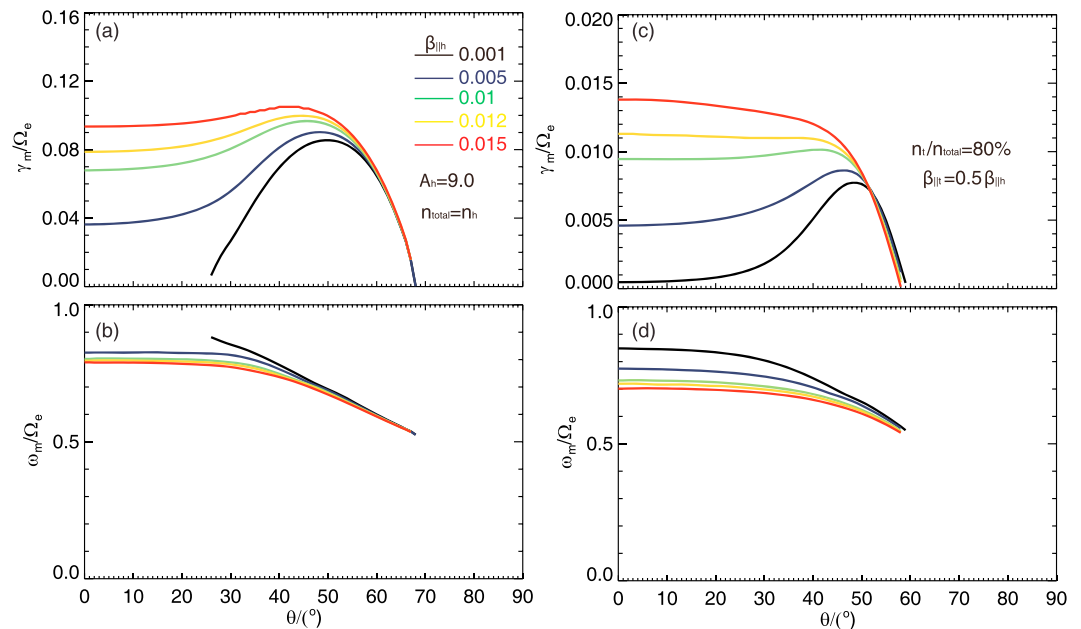


Figure 3. (a, c) The linear growth rate γ_m and (b, d) frequency ω_m as a function of wave normal angle for a series of cases with different parallel plasmas betas in the low-beta regime.

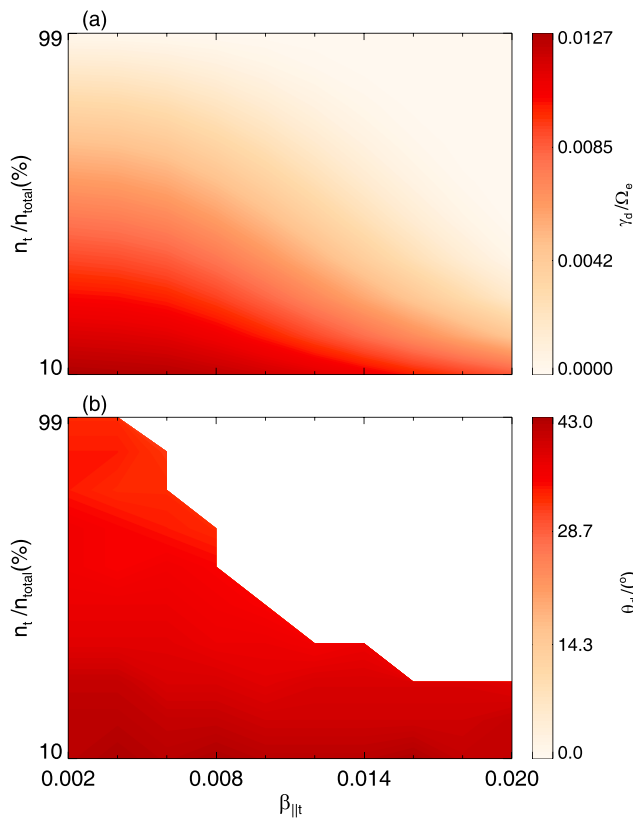


Figure 4. The distribution of (a) the linear growth rate γ_d and (b) wave normal angle θ_d of the dominant whistler mode in the $(\beta_{\parallel t}, n_t)$ plane in the low-beta regime.

this high-beta regime, which has also been pointed out by Gary et al. (2011). Their growth rates increase with the $\beta_{\parallel h}$ (Figure 1a), while their frequencies slightly decrease with the $\beta_{\parallel h}$ (Figure 1b). The effects of thermal electrons can be found in Figures 1c and 1d. First, the wave normal angle of the dominant wave mode for each case is still at 0° , but their growth rates become much smaller compared with cases only including hot electrons. This obvious reduction of growth rates is mainly caused by the lower percentage of hot anisotropic electrons. Second, the frequencies of unstable wave modes in all cases are found to decrease, and there is also a trend that the wave frequency is inversely correlated with the $\beta_{\parallel h}$.

The effects of thermal electrons on whistler modes in the high-beta regime are summarized in Figure 2, which displays the distribution of the linear growth rate γ_d in the $(\beta_{\parallel t}, n_t)$ plane. Hereafter, the subscript d denotes the dominant wave mode with the maximum growth rate in each case. Here the parallel plasma beta and anisotropy of hot electrons are fixed as $\beta_{\parallel h} = 0.2$ and $A_h = 2.25$, which are chosen without any preference in the high-beta regime. Just as discussed above, the growth rate of the dominant whistler mode is found to decrease with the increasing proportion of thermal electrons. Besides, with the increase of the plasma beta of thermal electrons, the growth rate also becomes smaller, which may be due to the stronger damping effect caused by thermal electrons with a higher temperature. It is worth noting that the wave normal angle of the dominant wave mode is still 0° , which is not affected by thermal electrons.

With a same format as Figure 1, Figure 3 presents several cases in the low-beta regime. For the cases only including anisotropic electrons, the dominant whistler modes turn out to be oblique with respect to the background magnetic field, with wave normal angle around 50° (Figure 3a). Their growth rates also increase with the plasma beta of anisotropic electrons.

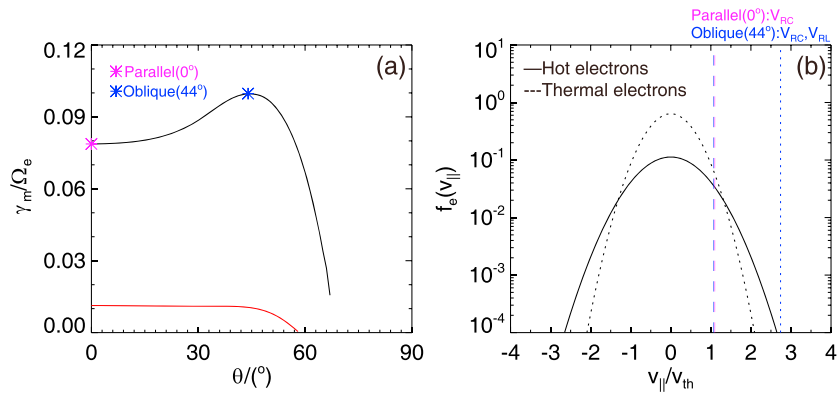


Figure 5. (a) The linear growth rate as a function of the wave normal for two cases (yellow curve in Figures 3a and 3c). The black curve denotes the case only containing anisotropic component, while the red curve represents the case containing both thermal and anisotropic components. The dominant wave mode for each case is marked by a star: magenta star for the parallel mode and blue star for the oblique mode. (b) The initial parallel velocity distributions of hot (black solid line) and thermal (black dotted line) components. The vertical lines mark the resonant velocities of two selected modes in panel a.

Since a high anisotropy is chosen here, then the frequencies of those dominant modes fall into the upper band. When there is a thermal component in the plasma system, the growth rates of all wave modes also significantly decrease (Figure 3c). What is interesting here is that the growth rates show varying degrees

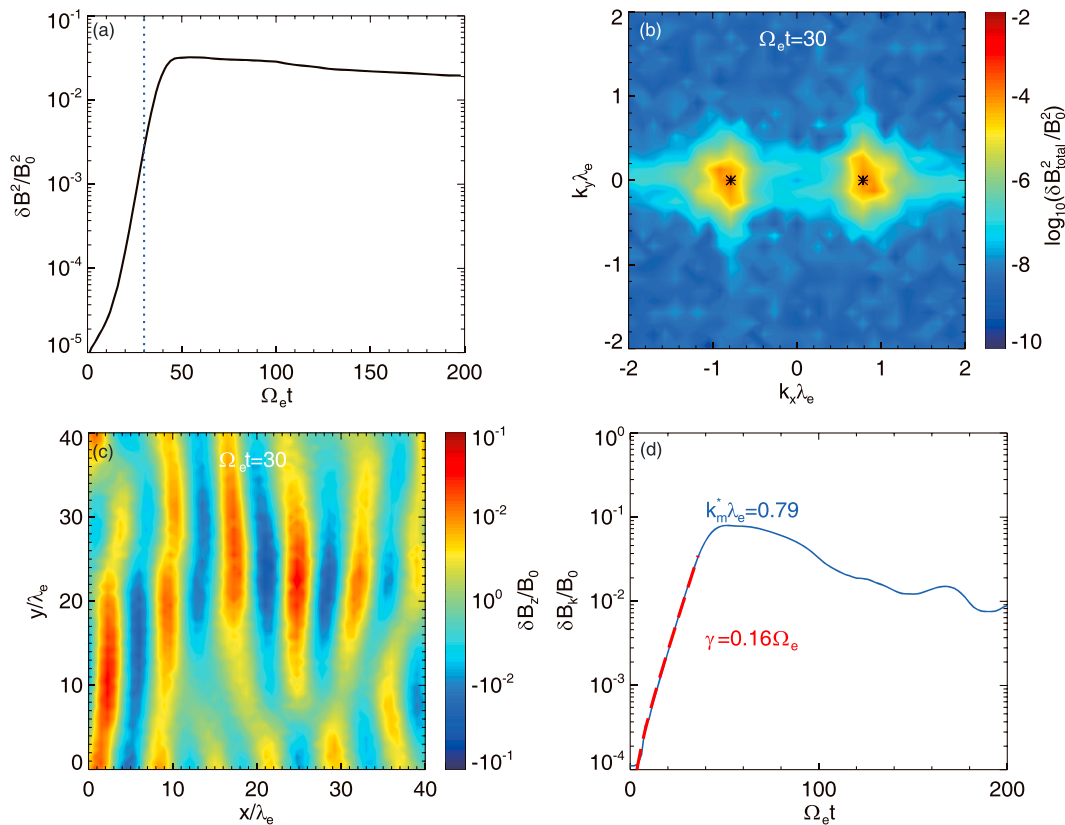


Figure 6. (a) The temporal profile of the intensity of fluctuating magnetic fields $\delta B^2 / B_0^2$, (b) the distribution of magnetic power $\delta B_{total}^2 / B_0^2$ in the (k_x, k_y) plane at $\Omega_e t = 30$, (c) the distribution of fluctuating magnetic fields $\delta B_z / B_0$ at $\Omega_e t = 30$, and (d) the temporal profile of the magnetic amplitude for the dominant wave mode marked by black stars “*” in panel b for Run 1. The time shown in panels b and c is corresponding to that marked by the blue dotted line in panel a. In panel d, the red dashed line represents the linear fit of $\delta B_k(t) / B_0$ in the linear growth phase.

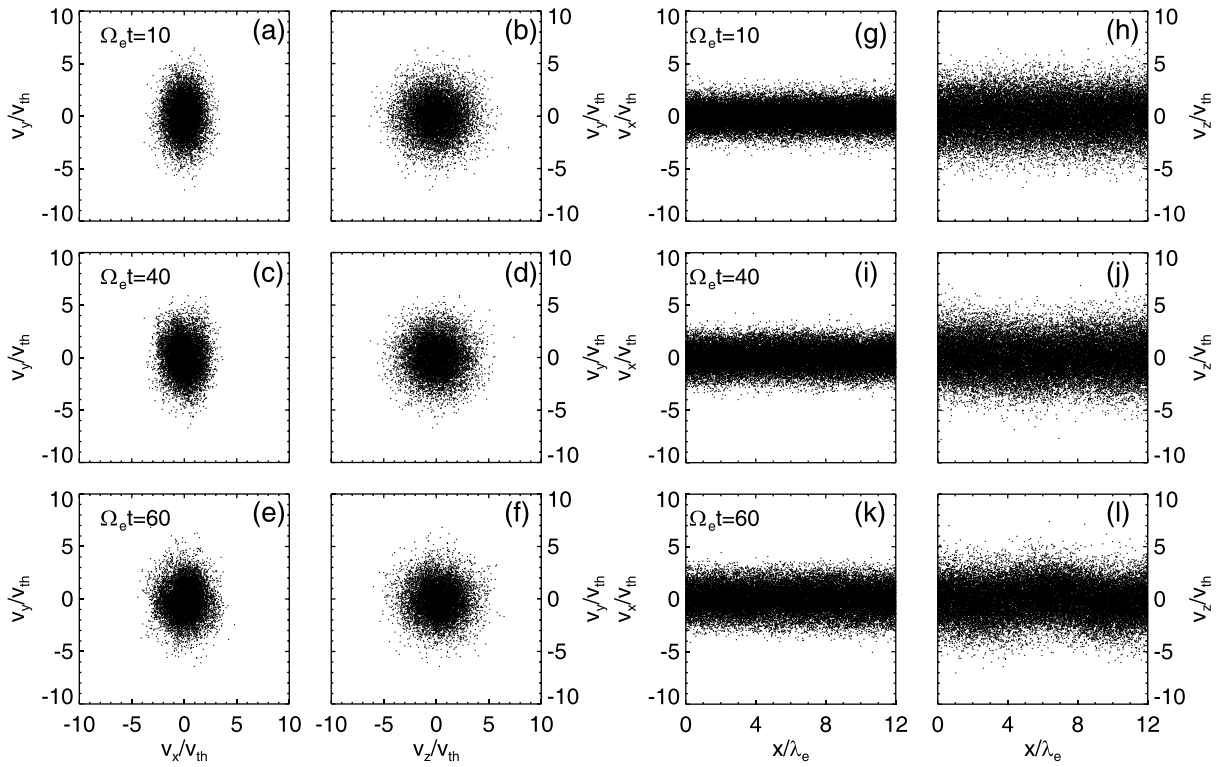


Figure 7. The scatterplots of electrons in the (v_x, v_y) plane (a, c, and e), (v_z, v_y) plane (b, d, and f), (x, v_x) plane (g, i, and k), and (x, v_z) plane (h, j, and l) at $\Omega_e t = 10, 40,$ and $60,$ respectively.

of decline for wave modes with different wave normal angles in each case. Specifically, the whistler mode with a larger wave normal angle ($>30^\circ$) experiences a more significant decrease of the linear growth rate. As a result, the dominant wave mode becomes parallel propagating in some cases, such as red and yellow curves in Figure 3c.

The effects of thermal electrons on the growth rate and wave normal angle of the dominant whistler mode in the low-beta regime are shown in Figure 4, which presents the distribution of (a) the linear growth rate γ_d and (b) wave normal angle θ_d of the dominant whistler mode in the $(\beta_{\parallel t}, n_r)$ plane. Note that the parallel plasma beta and anisotropy of hot electrons are fixed as $\beta_{\parallel h} = 0.02$ and $A_h = 3.78$, which are chosen without any preference in the low-beta regime. Similar to the cases in the high-beta regime (Figure 2), the linear growth rate is also inversely correlated with the plasma beta and density of thermal electrons (Figure 4a). In Figure 4b, the white area denotes that the dominant whistler mode is parallel propagating (i.e., $\theta_d = 0$) in those cases. Most notably, there is a clear turning point of the wave normal angle of the dominant wave mode with the increase of the $\beta_{\parallel t}$ and n_r . Specifically, the excited whistler mode tends to become parallel propagating from an oblique one with the increase of the $\beta_{\parallel t}$ and n_r . This indicates that the wave normal angle of whistler mode with the maximum growth rate is not only controlled by the plasma beta of anisotropic electrons but also modulated by thermal electrons. To better understand the change of wave normal angle, a further physical explanation is given in Figure 5. Taking two cases (yellow curve in Figures 3a and 3c) as examples, we have presented the linear growth rate as a function of the wave normal angle for two cases in Figure 5a. The black curve denotes the case only containing anisotropic component, and the wave normal angle of the dominant whistler mode is about 44° . While, the red curve represents the case containing both thermal and anisotropic components, and the dominant mode now becomes parallel propagating. We select these two modes (blue and magenta stars) to calculate their resonant velocities, which are shown in Figure 5 b. The parallel velocity distributions of hot and thermal components are denoted by the black solid and dotted lines, respectively. First, the Landau resonant velocity of the oblique wave is far away from the thermal population. Second, both parallel and oblique waves can interact with thermal electrons through the

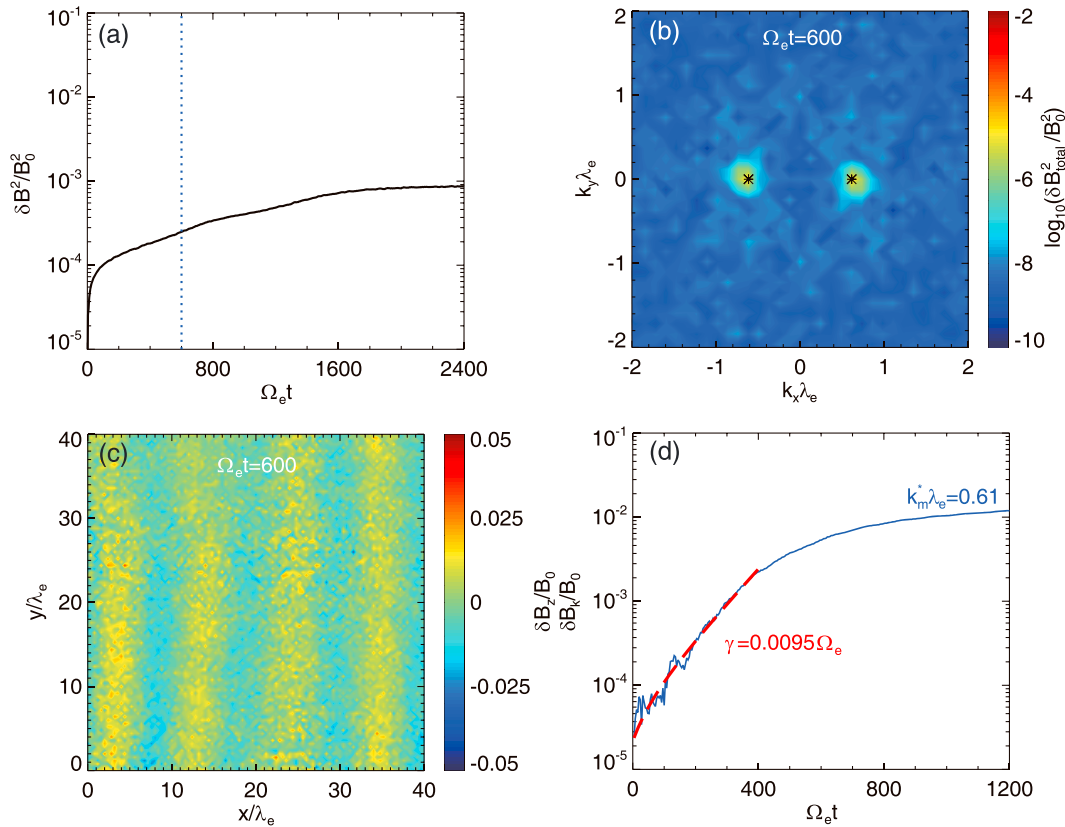


Figure 8. The simulation results for Run 2 in the same format as Figure 6.

cyclotron resonance, but the oblique wave has a smaller resonant velocity. This means that oblique waves experience stronger damping by thermal electrons, which could be the main reason that less oblique waves are excited in this case. To roughly estimate the damping rate of two wave modes caused by thermal electrons, we simply consider a plasma system only containing thermal component. With the WHAMP model, we calculate the growth rates for oblique ($k_{\parallel} \lambda_e \approx 2.40$, $k_{\perp} \lambda_e \approx 2.30$, and $\omega \approx 0.65 \Omega_e$) and parallel ($k_{\parallel} \lambda_e \approx 1.69$ and $\omega \approx 0.71 \Omega_e$) modes to be -0.0081 and $-0.0038 \Omega_e$. Note that the frequencies of two wave modes change due to the change of the dispersion relation of whistler modes. We can find that both modes are damped by thermal electrons, but the oblique mode experiences stronger damping.

3.2. PIC Simulations

With a 2-D PIC model, four runs listed in Table 1 are performed to further demonstrate the effects of thermal electrons on the generated whistler waves in a more self-consistent plasma system. Figure 6 gives the result for Run 1, including (a) the temporal profile of the intensity of fluctuating magnetic fields $\delta B^2/B_0^2$ ($\delta B^2 = \delta B_x^2 + \delta B_y^2 + \delta B_z^2$), (b) the distribution of total magnetic power $\delta B_{total}^2/B_0^2$ in the (k_x, k_y) plane at $\Omega_e t = 30$, (c) the distribution of fluctuating magnetic fields $\delta B_z/B_0$ at $\Omega_e t = 30$, and (d) the temporal profile of the magnetic amplitude $\delta B_k/B_0$ for the dominant wave mode marked by black stars “*” in panel b. Here the total magnetic power is the sum of the power of all three magnetic components. In Figures 6b and 6c, in order to compare with the results obtained from the linear theory, the time is chosen in the linear growth phase of fluctuating magnetic fields, which has been marked by the blue dotted line in Figure 6a. As shown in Figure 6a, the anisotropic hot electrons are unstable to excited whistler mode waves, which then saturate at $\sim 50 \Omega_e^{-1}$ after a linear growth phase. The dominant wave mode ($k_m^* \lambda_e \approx 0.79$) with the largest magnetic power is located at the parallel direction (Figure 6b), which is consistent with the prediction of the linear theory ($k_m \lambda_e = 0.8$) in this case. Moreover, the generated whistler waves actually exhibit a broad spectrum, which further result in the modulation of waveforms in both x and y directions (Figure 6c). In Figure 6d, at each time point, we

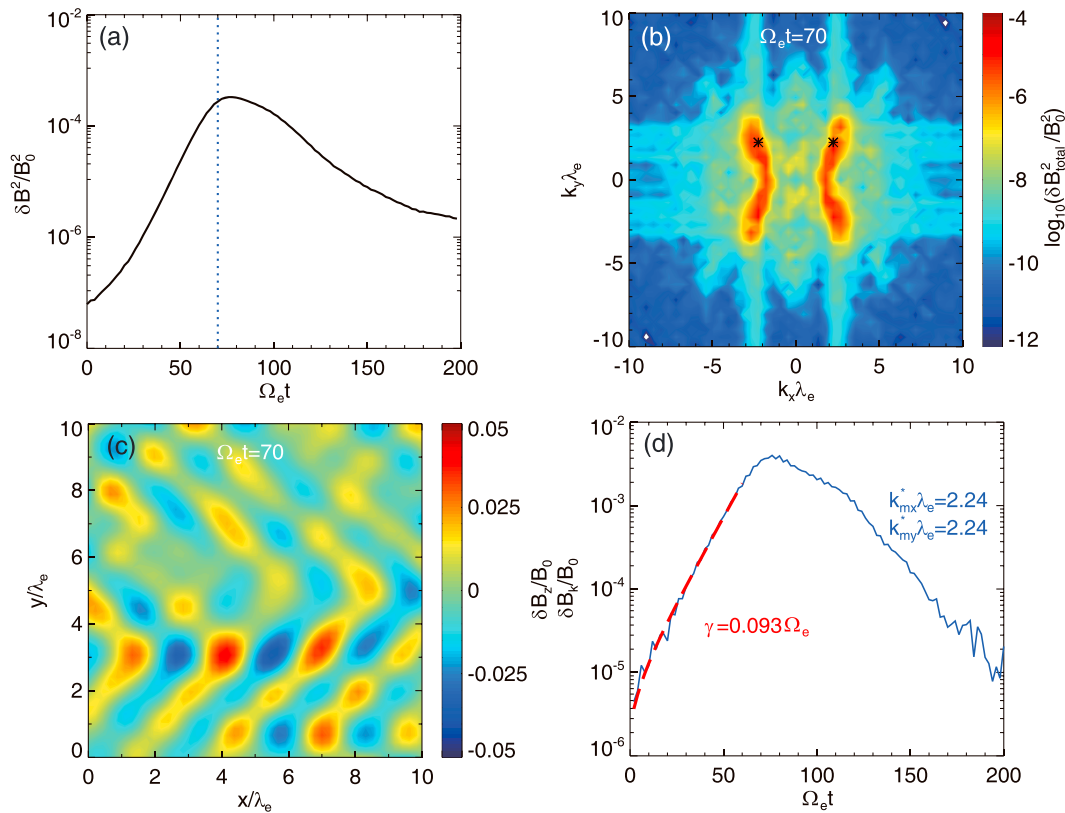


Figure 9. The simulation results for Run 3 in the same format as Figure 6.

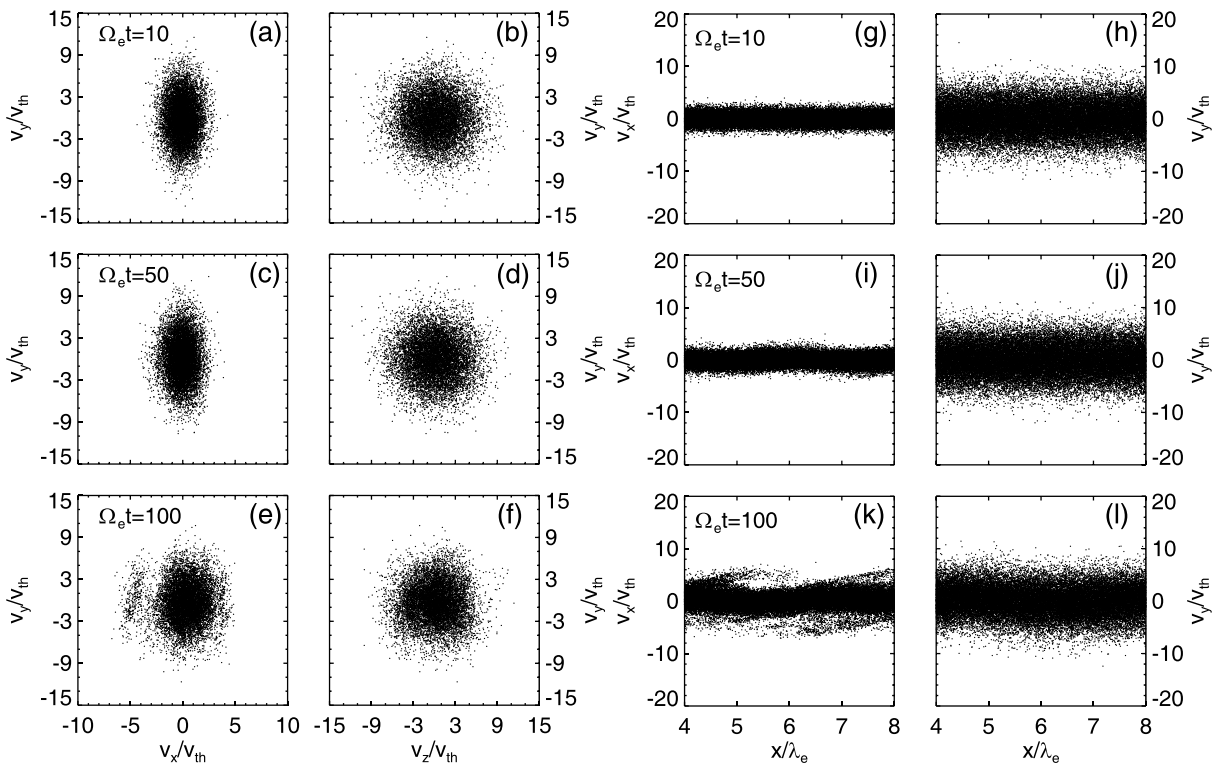


Figure 10. The scatterplots of electrons for Run 3 in the same format as Figure 7.

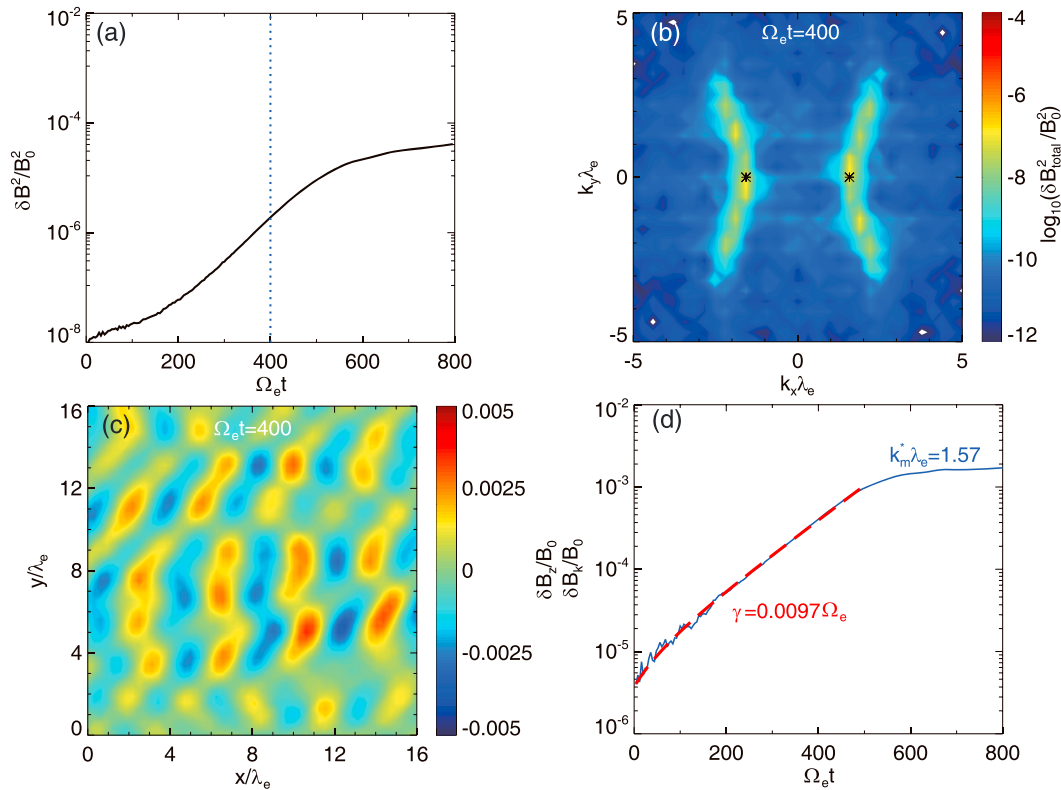


Figure 11. The simulation results for Run 4 in a same format as Figure 6.

first obtain the magnetic power spectrum in the (k_x, k_y) plane by performing the 2-D Fourier transform and then select the magnetic power at $k_m^* \lambda_e \approx 0.79$. Through a linear fit of $\delta B_k/B_0$ from 2 to $36\Omega_e^{-1}$, the growth rate of this dominant wave mode is estimated as $\sim 0.16\Omega_e$, which is quite similar to that given by the linear theory ($\gamma \approx 0.17\Omega_e$). We have also investigated the electron dynamics during the instability for Run 1. Figure 7 exhibits the scatterplots of hot electrons in the (v_x, v_y) plane (a, c, and e), (v_z, v_y) plane (b, d, and f), (x, v_x) plane (g, i, and k), and (x, v_z) plane (h, j, and l) at three different times. Most notably, the excited whistler mode waves scatter electrons into the parallel direction, resulting in the reduction of anisotropy (Figures 7c and 7e), and also the saturation of the instability. Meanwhile, the perpendicular bulk velocity of hot electrons fluctuates along the x axis (Figures 7j and 7l), which is consistently coupled with the wave fields.

With a same format, Figure 8 illustrates the results for Run 2, where 90% of electrons are thermal electrons. The growth rate of fluctuating magnetic fields is found to decrease so significantly, as well as the saturation amplitude (Figure 8a). The magnetic spectrum of excited whistler waves becomes very narrow but still peaks at the parallel direction (Figure 8b). Meanwhile, the fluctuating magnetic fields in Figure 8c depict four clear uniform waveforms. Compared with Run 1, the wave number and growth rate of the dominant wave mode in Run 2 decline to $0.61\lambda_e^{-1}$ and $0.0095\Omega_e$. In Run 2, the evolution of hot electrons is quite similar to that in Run 1, while thermal electrons are found to be slightly heated in the perpendicular direction (not shown).

The low-beta cases are also simulated. The results of Run 3 are displayed in Figure 9 in the same format as Figure 6. In this case, the parallel plasma beta of anisotropic electrons is very low (i.e., $\beta_{\parallel h} = 0.012$), which is in favor of generation of oblique whistler waves. Consistent with the linear theory, the dominant wave mode is found to have a wave normal angle of 45° (Figure 9b). Besides, those excited whistler waves show a very broad magnetic spectrum with a large range of wave normal angles from 0° to $\sim 50^\circ$. Since many waves modes are generated with different wave numbers, the waveforms shown in Figure 9c have been strongly modulated and are far from a sinusoidal pattern. Here the calculated growth rate of the dominant wave mode ($k_{mx}^* \lambda_e = 2.24$) is about $0.093\Omega_e$, which is quite similar to the value ($0.0997\Omega_e$) obtained from the

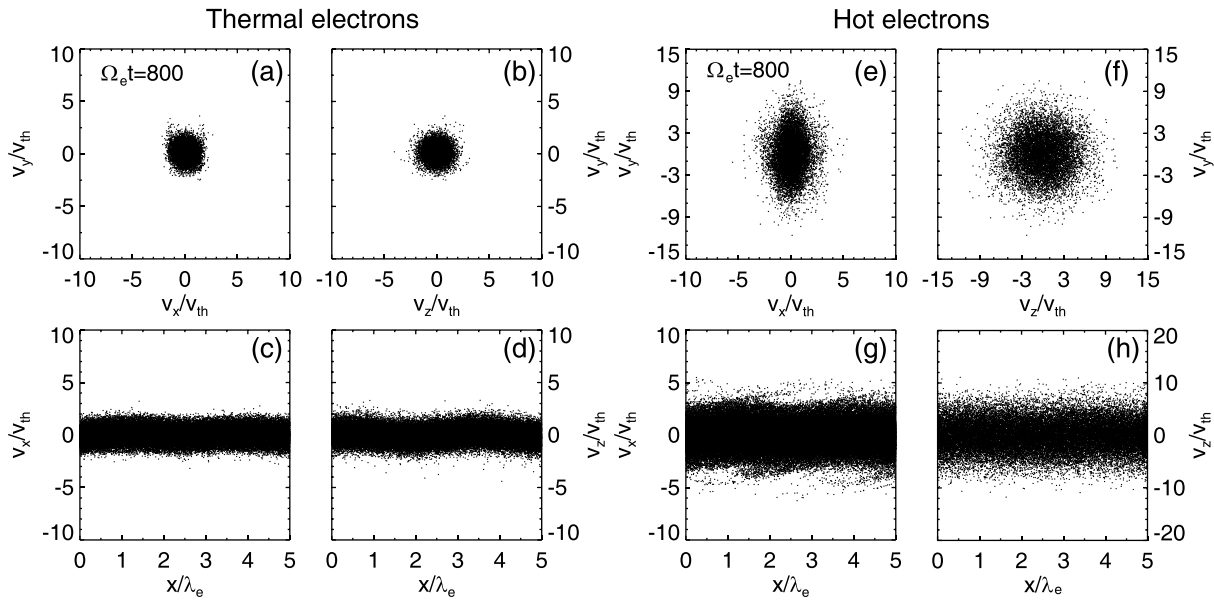


Figure 12. The scatterplots of electrons in the (v_x, v_y) plane (a and e), (v_z, v_y) plane (b and f), (x, v_x) plane (c and g), and (x, v_z) plane (d and h) for both thermal and hot components at $\Omega_e t = 800$.

linear theory. In the same format as Figure 7, Figure 10 presents the evolution of the electron distribution for Run 3. Expectedly, the anisotropy of electrons gradually decreases after the excitation of whistler mode waves, which is due to the scattering of electrons in the parallel direction (Figures 10c and 10e). Since the oblique whistler mode waves have the significant parallel electric fields, it is interesting to find that some electrons with large parallel velocities are trapped in the wave potential and accelerated in the parallel direction (Figures 10e and 10k).

Figure 11 gives the results of Run 4. In this low-beta case, the thermal electrons also reduce the growth and intensity of fluctuating magnetic fields (Figure 11a). Most notably, although the oblique whistler modes also appear in this system, the strongest mode now becomes nearly parallel propagating (Figure 11b), whose growth rate is calculated as $0.0097\Omega_e$ (Figure 11d). Figure 12 displays the scatterplots of electrons in the (v_x, v_y) plane (a and e), (v_z, v_y) plane (b and f), (x, v_x) plane (c and g), and (x, v_z) plane (d and h) for both thermal and hot components at $\Omega_e t = 800$. Although the oblique whistler mode waves are excited with lower amplitudes, there are still parts of hot electrons trapped and accelerated in the parallel direction (Figure 12g). Moreover, in Figure 12a, we can also find that some thermal electrons are resonantly accelerated in the perpendicular direction, which is consistent with the result shown in Figure 5b.

4. Conclusion and Discussion

In this paper, we have investigated the effects of thermal electrons on the whistler anisotropy instability using both the linear theory and 2D PIC simulations. In the high-beta ($\beta_{||h} \geq 0.025$) regime, the wave normal angle of the dominant whistler mode is always 0° , which is independent of thermal electrons, while its wave frequency and linear growth rate decrease with the density and temperature of thermal electrons. These results are also confirmed by PIC simulations. Moreover, we further find that the excited whistler spectrum becomes narrower, if there are sufficient thermal electrons in the plasma. In the low-beta ($\beta_{||h} \leq 0.025$) regime, with the increase of the density and temperature of thermal electrons, the wave normal angle of the dominant whistler mode jumps to zero from a large value. This change could be due to the stronger damping caused by thermal electrons for oblique whistler mode, since oblique wave usually has a smaller cyclotron resonant velocity than parallel wave. In the case with sufficient thermal electrons, the PIC simulation also presents a broad magnetic spectrum of generated whistler waves but with a smaller magnitude. Moreover, the maximum power is found not in an oblique direction, but in the parallel direction. Furthermore, thermal electrons with large parallel velocities are resonantly accelerated in the

perpendicular direction, while parts of hot electrons are trapped and accelerated in the parallel direction. This indicates that the wave normal angle of the dominant wave mode is not only controlled by the plasma beta of anisotropic electrons but also modulated by the density and temperature of thermal electrons.

Previous studies have indicated that the dominant whistler mode with the maximum growth rate is parallel propagating if $\beta_{\parallel h} > 0.025$, while the maximum growth rate shifts to oblique propagation if $\beta_{\parallel h} < 0.025$ (Gary et al., 2011). In a recent statistical study by Yue et al. (2016), the quasi-parallel and oblique lower band chorus waves are found roughly separated by the plasma beta (~ 0.025). However, there are still substantial quasi-parallel lower band whistler waves having very small wave normal angles associated with the low beta (< 0.025 ; Yue et al., 2016), which is difficult to understand by the linear theory if only anisotropic electrons are considered in the plasma. Actually, it is more realistic to consider at least two components of electrons (thermal and hot electrons) in the Earth's magnetosphere (Fu et al., 2014; Gao et al., 2014a; Li et al., 2010, 2016). According to our results, the existence of thermal electrons could reduce the transition value of the plasma beta, which can provide a potential explanation for those parallel chorus waves associated with a very low beta in the magnetosphere.

Acknowledgments

This work was supported by the NSFC grants 41774151, 41604128, 41631071, and 41474125; Youth Innovation Promotion Association of Chinese Academy of Sciences (2016395); Young Elite Scientists Sponsorship Program by CAST (2018QNR001); and Key Research Program of Frontier Sciences, CAS (QYZDJ-SSW-DQC010). Jun Guo also acknowledges the support by Shandong Provincial Natural Science Foundation (ZR2017MD012), China. All simulation data are archived in the <https://pan.baidu.com/s/1pqqLA8qGazk8DLRokJaiog> repository.

References

- Agapitov, O. V., Artemyev, A. V., Mourenas, D., Mozer, F. S., & Krasnoselskikh, V. (2015). Nonlinear local parallel acceleration of electrons through Landau trapping by oblique whistler mode waves in the outer radiation belt. *Geophysical Research Letters*, *42*, 10,140–10,149. <https://doi.org/10.1002/2015GL066887>
- An, X., Yue, C., Bortnik, J., Decyk, V., Li, W., & Thorne, R. M. (2017). On the parameter dependence of the whistler anisotropy instability. *Journal of Geophysical Research: Space Physics*, *122*, 2001–2009. <https://doi.org/10.1002/2017JA023895>
- Artemyev, A., Agapitov, O., Mourenas, D., Krasnoselskikh, V., Shastun, V., & Mozer, F. S. (2016). Oblique whistler-mode waves in the Earth's inner magnetosphere: Energy distribution, origins, and role in radiation belt dynamics. *Space Science Reviews*, *200*(1-4), 261–355. <https://doi.org/10.1007/s11214-016-0252-5>
- Artemyev, A. V., Vasiliev, A. A., Mourenas, D., Agapitov, O. V., Krasnoselskikh, V., Boscher, D., & Rolland, G. (2014). Fast transport of resonant electrons in phase space due to nonlinear trapping by whistler waves. *Geophysical Research Letters*, *41*, 5727–5733. <https://doi.org/10.1002/2014GL061380>
- Burtis, W. J., & Helliwell, R. A. (1969). Banded chorus a new type of VLF radiation observed in the magnetosphere by OGO 1 and OGO 3. *Journal of Geophysical Research*, *74*(11), 3002–3010. <https://doi.org/10.1029/JA074i011p03002>
- Chen, H., Gao, X., Lu, Q., Sun, J., & Wang, S. (2018). Nonlinear evolution of counter-propagating whistler mode waves excited by anisotropic electrons within the equatorial source region: 1-D PIC simulations. *Journal of Geophysical Research: Space Physics*, *123*, 1200–1207. <https://doi.org/10.1002/2017JA024850>
- Chen, H. Y., Gao, X. L., Lu, Q. M., Ke, Y. G., & Wang, S. (2017). Lower band cascade of whistler waves excited by anisotropic hot electrons: One-dimensional PIC simulations. *Journal of Geophysical Research: Space Physics*, *122*, 10,448–10,457. <https://doi.org/10.1002/2017JA024513>
- Chen, H. Y., Gao, X. L., Lu, Q. M., & Wang, S. (2018). In situ observations of harmonic alfvén waves and associated heavy ion heating. *The Astrophysical Journal*, *859*(2), 120. <https://doi.org/10.3847/1538-4357/aabee2>
- Denton, R. E. (2018). Electromagnetic ion cyclotron wavefields in a realistic dipole field. *Journal of Geophysical Research: Space Physics*, *123*, 1208–1223. <https://doi.org/10.1002/2017JA024886>
- Fu, X., Cowee, M. M., Friedel, R. H., Funsten, H. O., Peter Gary, S., Hospodarsky, G. B., et al. (2014). Whistler anisotropy instabilities as the source of banded chorus: Van Allen Probes observations and particle-in-cell simulations. *Journal of Geophysical Research: Space Physics*, *119*, 8288–8298. <https://doi.org/10.1002/2014JA020364>
- Fu, X. R., Gary, S. P., Reeves, G. D., Winske, D., & Woodroffe, J. R. (2017). Generation of highly oblique lower-band chorus via nonlinear three-wave resonance. *Geophysical Research Letters*, *44*, 9532–9538. <https://doi.org/10.1002/2017GL074411>
- Gao, X., Mourenas, D., Li, W., Artemyev, A. V., Lu, Q. M., Tao, X., & Wang, S. (2016). Observational evidence of generation mechanisms for very oblique lower band chorus using THEMIS waveform data. *Journal of Geophysical Research: Space Physics*, *121*, 6732–6748. <https://doi.org/10.1002/2016JA022915>
- Gao, X. L., Ke, Y. G., Lu, Q. M., Chen, L. J., & Wang, S. (2017). Generation of multiband chorus in the Earth's magnetosphere: 1-D PIC simulation. *Geophysical Research Letters*, *44*, 618–624. <https://doi.org/10.1002/2016GL072251>
- Gao, X. L., Li, W., Thorne, R. M., Bortnik, J., Angelopoulos, V., Lu, Q. M., et al. (2014b). Statistical results describing the bandwidth and coherence coefficient of whistler mode waves using THEMIS waveform data. *Journal of Geophysical Research: Space Physics*, *119*, 8992–9003. <https://doi.org/10.1002/2014JA020158>
- Gao, X. L., Li, W., Thorne, R. M., Bortnik, J., Angelopoulos, V., Lu, Q. M., et al. (2014a). New evidence for generation mechanisms of discrete and hiss-like whistler mode waves. *Geophysical Research Letters*, *41*, 4805–4811. <https://doi.org/10.1002/2014GL060707>
- Gao, X. L., Lu, Q. M., Bortnik, J., Li, W., Chen, L. J., & Wang, S. (2016). Generation of multiband chorus by lower band cascade in the Earth's magnetosphere. *Geophysical Research Letters*, *43*, 2343–2350. <https://doi.org/10.1002/2016GL068313>
- Gao, X. L., Lu, Q. M., & Wang, S. (2017). First report of resonant interactions between whistler mode waves in the Earth's magnetosphere. *Geophysical Research Letters*, *44*, 5269–5275. <https://doi.org/10.1002/2017GL073829>
- Gao, X. L., Lu, Q. M., Wang, S. J., & Wang, S. (2018). Theoretical analysis on lower band cascade as a mechanism for multiband chorus in the Earth's magnetosphere. *AIP Advances*, *8*, 055003. <https://doi.org/10.1063/1.5025507>
- Gary, S. P., Liu, K., & Winske, D. (2011). Whistler anisotropy instability at low electron: Particle-in-cell simulations. *Physics of Plasmas*, *18*(8), 082902. <https://doi.org/10.1063/1.3610378>
- Ke, Y. G., Gao, X., Lu, Q., Hao, Y., & Wang, S. (2018). Parametric decay of oblique whistler waves in the Earth's magnetosphere: 2-D PIC simulations. *Physics of Plasmas*, *25*, 072901. <https://doi.org/10.1063/1.5037763>

- Ke, Y. G., Gao, X., Lu, Q., Wang, X., & Wang, S. (2017). Generation of rising-tone chorus in a two-dimensional mirror field by using the general curvilinear PIC code. *Journal of Geophysical Research: Space Physics*, *122*, 8154–8165. <https://doi.org/10.1002/2017JA024178>
- Lauben, D. S., Inan, U. S., Bell, T. F., & Gurnett, D. A. (2002). Source characteristics of ELF/VLF chorus. *Journal of Geophysical Research*, *107*(A12), 1429. <https://doi.org/10.1029/2000JA003019>
- LeDocq, M. J., Gurnett, D. A., & Hospodarsky, G. B. (1998). Chorus source locations from VLF Poynting flux measurements with the Polar spacecraft. *Geophysical Research Letters*, *25*(21), 4063–4066. <https://doi.org/10.1029/1998GL900071>
- Li, W., Bortnik, J., Thorne, R. M., Cully, C. M., Chen, L., Angelopoulos, V., et al. (2013). Characteristics of the Poynting flux and wave normal vectors of whistler-mode waves observed on THEMIS. *Journal of Geophysical Research: Space Physics*, *118*, 1461–1471. <https://doi.org/10.1002/jgra.50176>
- Li, W., Mourenas, D., Artemyev, A. V., Agapitov, O. V., Bortnik, J., Albert, J. M., et al. (2014). Evidence of stronger pitch angle scattering loss caused by oblique whistler-mode waves as compared with quasi-parallel waves. *Geophysical Research Letters*, *41*, 6063–6070. <https://doi.org/10.1002/2014GL061260>
- Li, W., Mourenas, D., Artemyev, A. V., Bortnik, J., Thorne, R. M., Kletzing, C. A., et al. (2016). Unraveling the excitation mechanisms of highly oblique lower band chorus waves. *Geophysical Research Letters*, *43*, 8867–8875. <https://doi.org/10.1002/2016GL070386>
- Li, W., Thorne, R. M., Bortnik, J., Tao, X., & Angelopoulos, V. (2012). Characteristics of hiss-like and discrete whistler-mode emissions. *Geophysical Research Letters*, *39*, L18106. <https://doi.org/10.1029/2012GL053206>
- Li, W., Thorne, R. M., Nishimura, Y., Bortnik, J., Angelopoulos, V., McFadden, J. P., et al. (2010). THEMIS analysis of observed equatorial electron distributions responsible for the chorus excitation. *Journal of Geophysical Research*, *115*, A00F11. <https://doi.org/10.1029/2009JA014845>
- Lu, Q. M., Wang, L. Q., Zhou, Y., & Wang, S. (2004). Electromagnetic instabilities excited by electron temperature anisotropy. *Chinese Physics Letters*, *21*, 129–132.
- Lu, Q. M., Zhou, L. H., & Wang, S. (2010). Particle-in-cell simulations of whistler waves excited by an electron κ distribution in space plasma. *Journal of Geophysical Research*, *115*, A02213. <https://doi.org/10.1029/2009JA014580>
- Mourenas, D., Artemyev, A. V., Ripoll, J.-F., Agapitov, O. V., & Krasnoselskikh, V. V. (2012). Timescales for electron quasi-linear diffusion by parallel and oblique lower-band chorus waves. *Journal of Geophysical Research*, *117*, A06234. <https://doi.org/10.1029/2012JA017717>
- Ni, B., Thorne, R. M., Shprits, Y. Y., & Bortnik, J. (2008). Resonant scattering of plasma sheet electrons by whistler-mode chorus: Contribution to diffuse auroral precipitation. *Geophysical Research Letters*, *35*, L11106. <https://doi.org/10.1029/2008GL034032>
- Ni, B. B., Thorne, R. M., Shprits, Y. Y., Orlova, K. G., & Meredith, N. P. (2011). Chorus-driven resonant scattering of diffuse auroral electrons in nondipolar magnetic fields. *Journal of Geophysical Research*, *116*, A06225. <https://doi.org/10.1029/2011JA016453>
- Nishimura, Y., Bortnik, J., Li, W., Thorne, R. M., Ni, B., Lyons, L. R., et al. (2013). Structures of dayside whistler-mode waves deduced from conjugate diffuse aurora. *Journal of Geophysical Research: Space Physics*, *118*, 664–673. <https://doi.org/10.1029/2012JA018242>
- Ratcliffe, H., & Watt, C. E. J. (2017). Self-consistent formation of a 0.5 cyclotron frequency gap in magnetospheric whistler mode waves. *Journal of Geophysical Research: Space Physics*, *122*, 8166–8180. <https://doi.org/10.1002/2017JA024399>
- Reeves, G. D., Spence, H. E., Henderson, M. G., Morley, S. K., Friedel, R. H. W., Funsten, H. O., et al. (2013). Electron acceleration in the heart of the Van Allen radiation belts. *Science*, *341*(6149), 991–994. <https://doi.org/10.1126/science.1237743>
- Ronnmark, K. (1982). WHAMP: Waves in homogeneous, anisotropic, multicomponent plasmas, Kiruna Geophysical Institute, Report 179. Kiruna, Sweden.
- Santolik, O., Gurnett, D. A., Pickett, J. S., Chum, J., & Cornilleau-Wehrin, N. (2009). Oblique propagation of whistler mode waves in the chorus source region. *Journal of Geophysical Research*, *114*, A00F03. <https://doi.org/10.1029/2009JA014586>
- Santolik, O., Gurnett, D. A., Pickett, J. S., Parrot, M., & Cornilleau-Wehrin, N. (2005). Central position of the source region of storm-time chorus. *Planetary and Space Science*, *53*(1–3), 299–305. <https://doi.org/10.1016/j.pss.2004.09.056>
- Shprits, Y. Y., & Ni, B. (2009). Dependence of the quasi-linear scattering rates on the wave normal distribution of chorus waves. *Journal of Geophysical Research*, *114*, A11205. <https://doi.org/10.1029/2009JA014223>
- Thorne, R. M., Li, W., Ni, B., Ma, Q., Bortnik, J., Chen, L., et al. (2013). Rapid local acceleration of relativistic radiation-belt electrons by magnetospheric chorus. *Nature*, *504*(7480), 411–414. <https://doi.org/10.1038/nature12889>
- Thorne, R. M., Ni, B., Tao, X., Horne, R. B., & Meredith, N. P. (2010). Scattering by chorus waves as the dominant cause of diffuse auroral precipitation. *Nature*, *467*(7318), 943–946. <https://doi.org/10.1038/nature09467>
- Tsurutani, B. T., & Smith, E. J. (1974). Postmidnight chorus: A substorm phenomenon. *Journal of Geophysical Research*, *79*(1), 118–127. <https://doi.org/10.1029/JA079i001p00118>
- Xiao, F., Chen, L., Zheng, H., & Wang, S. (2007). A parametric ray tracing study of superluminous auroral kilometeric radiation wave modes. *Journal of Geophysical Research*, *112*, A10214. <https://doi.org/10.1029/2006JA012178>
- Xiao, F., Yang, C., He, Z., Su, Z., Zhou, Q., He, Y., et al. (2014). Chorus acceleration of radiation belt relativistic electrons during March 2013 geomagnetic storm. *Journal of Geophysical Research: Space Physics*, *119*, 3325–3332. <https://doi.org/10.1002/2014JA019822>
- Yue, C., An, X., Bortnik, J., Ma, Q., Li, W., Thorne, R. M., et al. (2016). The relationship between the macroscopic state of electrons and the properties of chorus waves observed by the Van Allen Probes. *Geophysical Research Letters*, *43*, 7804–7812. <https://doi.org/10.1002/2016GL070084>